Development of White Matter Hyperintensity Is Preceded by Reduced Cerebrovascular Reactivity

Kevin Sam, PhD,[1,2] Adrian P. Crawley, PhD,[2,3,4] John Conklin, MD, MSc,[2] Julien Poublanc, MSc,[2] Olivia Sobczyk, MSc,[2,4] Daniel M. Mandell, MD, PhD,[2,4] Lakshmikumar Venkatraghavan, MD,[5] James Duffin, PhD,[1,5] Joseph A. Fisher, MD,[1,4,5] Sandra E. Black, MD,[4,6] and David J. Mikulis, MD[2,3,4]

Objective: White matter hyperintensities (WMH) observed on neuroimaging of elderly individuals are associated with cognitive decline and disability. However, the pathogenesis of WMH remains poorly understood. We observed that regions of reduced cerebrovascular reactivity (CVR) in the white matter of young individuals correspond to the regions most susceptible to WMH in the elderly. This finding prompted us to consider that reduced CVR may play a role in the pathogenesis of WMH. We hypothesized that reduced CVR precedes development of WMH.
Methods: We examined 45 subjects (age range = 50–91 years; 25 males) with moderate–severe WMH, and measured their baseline CVR using the blood oxygen level–dependent magnetic resonance imaging signal response to a standardized step change in the end-tidal partial pressure of carbon dioxide. Diffusion tensor imaging and transverse relaxation time (T2) relaxometry were performed at baseline and 1-year follow-up, with automated coregistration between time points. Baseline fractional anisotropy (FA), mean diffusivity (MD), T2, and CVR were measured in areas that progressed from normal-appearing white matter (NAWM) to WMH over the 1-year period.
Results: CVR and FA values in baseline NAWM that progressed to WMH were lower by mean (standard deviation) = 26.5% (23.2%) and 11.0% (7.2%), respectively, compared to the contralateral homologous NAWM that did not progress ($p < 0.001$). T2 and MD were higher by 8.7% (7.9%) and 17.0% (8.5%), respectively, compared to the contralateral homologous NAWM ($p < 0.001$).
Interpretation: Areas of reduced CVR precede the progression from NAWM to WMH, suggesting that hemodynamic impairment may contribute to the pathogenesis and progression of age-related white matter disease.

ANN NEUROL 2016;80:277–285

In 1986, Hachinski et al[1] introduced the term leukoaraiosis ("leuko" = white, "araios" = rarefied) to describe the patchy areas of high transverse relaxation time (T2)-weighted magnetic resonance imaging (MRI) signals frequently observed in elderly individuals. However, the term leukoaraiosis is purely descriptive, intended only to describe these imaging findings without connotation of a specific pathophysiological process. By contrast, the STRIVE (STandards for ReportIng Vascular changes on nEuroimaging) consensus statement advocates the term "white matter hyperintensities of presumed vascular origin" if a vascular etiology is suspected.[2] Although these white matter hyperintensities (WMH) were once thought to represent benign age-related changes, they have now been shown to correlate strongly with cognitive impairment,[3] dementia,[4,5] and disability.[6,7] Given the high prevalence of WMH in the elderly,[8,9] it is important to understand its pathogenesis to propose and evaluate strategies for prevention and treatment.

Cerebrovascular reactivity (CVR) is defined as the change in flow in response to a vasoactive stimulus, and

View this article online at wileyonlinelibrary.com. DOI: 10.1002/ana.24712

Received Apr 13, 2016, and in revised form Jun 6, 2016. Accepted for publication Jun 26, 2016.

Address correspondence to Dr Mikulis, Toronto Western Hospital, Joint Department of Medical Imaging, McLaughlin Pavilion, 3rd Floor Room 431, 399 Bathurst St, Toronto, ON M5T 2S8, Canada. E-mail: mikulis@uhnres.utoronto.ca

From the [1]Department of Physiology, University of Toronto, Toronto, Ontario, Canada; [2]Division of Neuroradiology, Joint Department of Medical Imaging, University Health Network, Toronto, Ontario, Canada; [3]Department of Medical Imaging, University of Toronto, Toronto, Ontario, Canada; [4]Institute of Medical Sciences, University of Toronto, Toronto, Ontario, Canada; [5]Department of Anesthesiology, University Health Network, Toronto, Ontario, Canada; and [6]LC Campbell Cognitive Neurology Research Unit, Sunnybrook Health Sciences Centre, Toronto, Ontario, Canada

is a measure of the ability of the cerebral vasculature to control vascular resistance.[10] CVR measurements have the potential to reveal areas of hemodynamic insufficiency, where redistribution of flow occurs during a vasodilatory stimulus from areas of exhausted vasodilatory capacity to areas with a robust vasodilatory response.[10] A quantitative approach to measuring CVR has been validated for clinical evaluation[11] that uses the blood oxygen level–dependent (BOLD) MRI response to an accurately controlled hypercapnic stimulus. Two important findings suggest that chronic hemodynamic insufficiency may be implicated in the pathogenesis of WMH, specifically: (1) the mean CVR of WMH is diminished and is approximately half of that found in normal-appearing white matter (NAWM)[12]; and (2) the CVR of NAWM in young healthy individuals is diminished[13] in a pattern that spatially corresponds to predilection maps of WMH in the elderly.[14] It is unknown whether WMH causes reduced CVR due to decreased metabolic demand or whether reductions in CVR lead to the development of WMH. This study examined the possible relationship between diminished CVR and the progression from NAWM to WMH.

In addition to CVR, diffusion tensor imaging (DTI) has been shown to be sensitive to subtle white matter structural changes in NAWM.[15,16] A serial DTI and quantitative T2 MRI study followed subjects with age-related WMH over 16 weeks and found abnormally low fractional anisotropy (FA), high mean diffusivity (MD), and high T2 values in de novo WMH.[17] Another study that prospectively investigated WMH progression over 3.5 years found lower baseline FA and higher baseline MD in NAWM that progressed to WMH.[18] Whether reduced CVR precedes the progression of NAWM to WMH is not known. To answer this question, we examined 45 subjects with age-related WMH using 2 multiparametric MRI scans 1 year apart to evaluate the temporal evolution of structural and hemodynamic parameters of the white matter. We hypothesize that NAWM that progresses to WMH will demonstrate reduced baseline CVR and alterations in structural MRI parameters when compared to NAWM that remains stable over time.

Patients and Methods

Subject Recruitment and Assessment

This study was conducted at the Toronto Western Hospital (TWH) and Sunnybrook Health Sciences Centre (SHSC). Subjects were recruited through outpatient neurology clinics at both sites. Subjects were initially referred by their family physicians to neurology clinics because of syncopal episodes, transient paresthesia, gait disturbances, headaches, memory impairment, or cognitive decline. Magnetic resonance angiogram/computed tomographic angiography of the head and neck as well as T2-weighted fluid-attenuated inversion recovery (FLAIR) images were screened by 2 experienced neuroradiologists (D.M.M. and D.J.M), and subjects were enrolled in the study based on the following criteria: (1) imaging evidence of acute neurological event on diffusion-weighted imaging in the white matter must be >3 months from presentation prior to study enrolment; (2) older than 50 years; (3) MRI white matter disease burden ≥ Fazekas grade 2[19]; (4) no evidence of hemodynamically significant (ie, > 50%) internal carotid artery or vertebrobasilar stenosis; (5) no evidence of arterial dissection; (6) no prior large cortical infarct > 2cm or cavitary white matter lesion > 2cm; (7) no history or clinical evidence of pulmonary or cardioembolic disease; (8) no contraindication to 3T MRI; and (9) must not be on medications known to alter CVR, including nitrates and calcium channel blockers.

Forty-five elderly adults (age range = 50–91 years; 25 males) were recruited and provided written informed consent to procedures approved by the respective institutional ethics review boards in accordance with the 1964 Declaration of Helsinki (see Table 1 for patient characteristics).

TABLE 1. Baseline Characteristics of Subjects

Parameter	Value
Demographics	
Age, yr, mean (SD)	74 (9.4)
Men, No. [%]	25 [56]
Baseline WMH volume, ml (SD)	32 (25)
MoCA, mean (SD), 6 missing values	25 (4)
Vascular risk factors, No. [%]	
Ischemic stroke	12 [27]
Transient ischemic attack	6 [13]
Coronary artery disease	7 [16]
Hypertension	23 [51]
Hypercholesterolemia	19 [42]
Diabetes mellitus	3 [7]
Current smoking	3 [7]
Obstructive sleep apnea	5 [11]

Total n = 45.
MoCA = Montreal Cognitive Assessment. SD = standard deviation.

Image Acquisition

Subjects underwent MRI scans on a 3T GE system (Signa HDx platform; GE Healthcare, Milwaukee, WI) at TWH and 3T Philips Achieva system (Philips Medical Systems, Best, the Netherlands) at SHSC with an 8-channel phased array head coil. Subjects were asked to refrain from heavy exercise and

drinking caffeine on the day of each scan. The imaging acquisition parameters are listed from SHSC to TWH as follows: T1-weighted 3-dimensional spoiled gradient-echo sequence (slice thickness = 1.2 to 1.5mm; no interslice gap; matrix size = 256 × 256; field of view = 22 × 22cm; flip angle = 8 to 20°; echo time [TE] = 2.3 to 3 milliseconds; repetition time [TR] = 7.8 to 9.5 milliseconds), BOLD functional MRI using a T2*-weighted echo-planar imaging gradient-echo sequence (slice thickness = 3.0 to 5.0mm; field of view = 24 × 24cm; matrix size = 64 × 64; flip angle = 85 to 90°; TE = 30 milliseconds; TR = 2,000 milliseconds), conventional FLAIR images (slice thickness = 3mm; 36 to 52 slices per volume; no interslice gap; matrix size = 256 × 224 to 240 × 240; field of view = 22 × 22cm; flip angle = 90°; TE = 125 to 165 milliseconds; TR = 9,000 to 9,145 milliseconds; inversion time- = 2,200 to 2,800 milliseconds); DTI with an echo-planar imaging spin-echo sequence (slice thickness = 3mm; matrix size = 76 × 62 to 128 × 128; field of view = 22 × 22cm; b = 1,000 s/mm^2; 23 diffusion-encoding gradients; 2 non–diffusion-weighted B0 images; TE = 55 to 80 milliseconds; TR = 9,150 to 14,500 milliseconds); proton density/T2-weighted images using fast spin-echo-XL (slice thickness = 3mm; no interslice gap; matrix size = 128 × 128 to 256 × 209; field of view = 22 × 22cm; flip angle = 90°; TE = 11.1/90 to 11/102 milliseconds; TR = 2,500 to 7,200 milliseconds), and multiecho T2 mapping using a fast spin-echo-XL sequence (slice thickness = 3mm; no interslice gap; matrix size = 256 × 192; field of view = 230 × 184 to 22 × 22cm; TE = 13, 26, 39, 52, 65, 78, 91, 104, 117, 130, 143, 156 milliseconds; TR = 5,000 to 6,000 milliseconds).

Vasodilatory Stimulus (Gas Manipulation, End-Tidal pCO_2, and pO_2 Manipulation)

Control of the end-tidal partial pressure of CO_2 ($P_{ET}CO_2$) and O_2 ($P_{ET}O_2$) was achieved using an automated gas blender that adjusts gas composition and flow to a sequential gas delivery breathing circuit (RespirAct; Thornhill Research, Toronto, Canada). This allows $P_{ET}CO_2$ and $P_{ET}O_2$ to be controlled independent of the subject's ventilation and breathing pattern.[20,21] The system operation and implementation of $P_{ET}CO_2$ and $P_{ET}O_2$ sequences used during the analysis of BOLD CVR are described in detail elsewhere.[22–24] The vasodilatory stimulus used in this study was as follows: a baseline $P_{ET}CO_2$ of 40mmHg for 60 seconds (normocapnia), followed by an abrupt hypercapnic step change to $P_{ET}CO_2$ of 50mmHg for 90 seconds, then a return to baseline for 90 seconds, followed by a second abrupt hypercapnic step change for 120 seconds, with a final return to baseline.[25] Normoxia ($P_{ET}O_2$ = ~110mmHg) was maintained throughout.

Image Reconstruction

The acquired BOLD MRI and $P_{ET}CO_2$ data were imported to AFNI[26] for analysis. BOLD images were slice time-corrected, volume-registered, and aligned to axial anatomical T1-weighted images. The CVR maps were then constructed by first time-shifting the acquired $P_{ET}CO_2$ data to the point of maximum correlation with the whole brain average BOLD signal using MATLAB software (MathWorks, Natick, MA), to compensate for the transit time delay from pulmonary to cerebral circulation. Then, a voxel-by-voxel linear least-squares fit of the BOLD signal time series to the $P_{ET}CO_2$ data (regressor) was performed and the slope of the line of best fit was taken as CVR.

Quantitative T2 maps were obtained using multiecho fast spin-echo images. T2 maps were calculated in AFNI using methods previously described.[27] To calculate FA and MD maps, diffusion-weighted images were imported into FSL 4.1.8.[28] Preprocessing included eddy current and motion artifact correction using FMRIB's Diffusion Toolbox (FDT).[29] Next, individual brain masks were created using FSL's Brain Extraction Tool.[30] The preprocessed images were fit with a diffusion tensor model using DTIFIT in FDT.[28]

CVR Measurement

CVR was assessed by measuring the change in BOLD MRI signal in response to changes in the end-tidal (ie, end-expiratory) $P_{ET}CO_2$, and defined as ΔBOLD signal (%)/Δ$P_{ET}CO_2$ (mmHg). A color scale ranging from blue to red was used to illustrate the magnitude of CVR, with negative CVR values interpreted as "steal physiology" shown as shades of blue, and positive CVR values are shown as shades of yellow, orange, and red (Fig 1).

Generating Regions of Interest of NAWM and WMH

Segmentation of WMH was performed using the Lesion Explorer processing pipeline based on FLAIR, proton density (PD), and T2-weighted images (available for download at http://sabre.brainlab.ca).[31,32] These images were reviewed to identify newly appearing lesions. Lesion Explorer was used to obtain measures of supratentorial total intracranial volume (total brain tissue and cerebrospinal fluid). A region of interest (ROI) encompassing all newly developed lesions was manually traced using AFNI.[26] T1-weighted anatomical images were segmented into cerebrospinal fluid, gray matter, and white matter using SPM8 (Wellcome Department of Imaging Neuroscience, Institute of Neurology, University College, London, UK). Gray matter and white matter volumes were normalized for total intracranial volume. A diamond-shaped structuring element was used to erode the white matter segmentation in 5 iterations at the resolution of the T1-weighted image to prevent partial voluming effects. WMH were subtracted after erosion to give rise to a NAWM mask.

Spatial Factor Corrected Regional Measures

White matter CVR is spatially heterogeneous in healthy subjects,[13] so it is possible that observed differences between regions of white matter in our subjects are due to this normal spatial variation rather than tissue pathology. For example, WMH tend to develop in the periventricular white matter and CVR may also be intrinsically lower in these areas. Therefore, CVR differences between NAWM and de novo WMH may produce false-positive results. To account for spatial location,

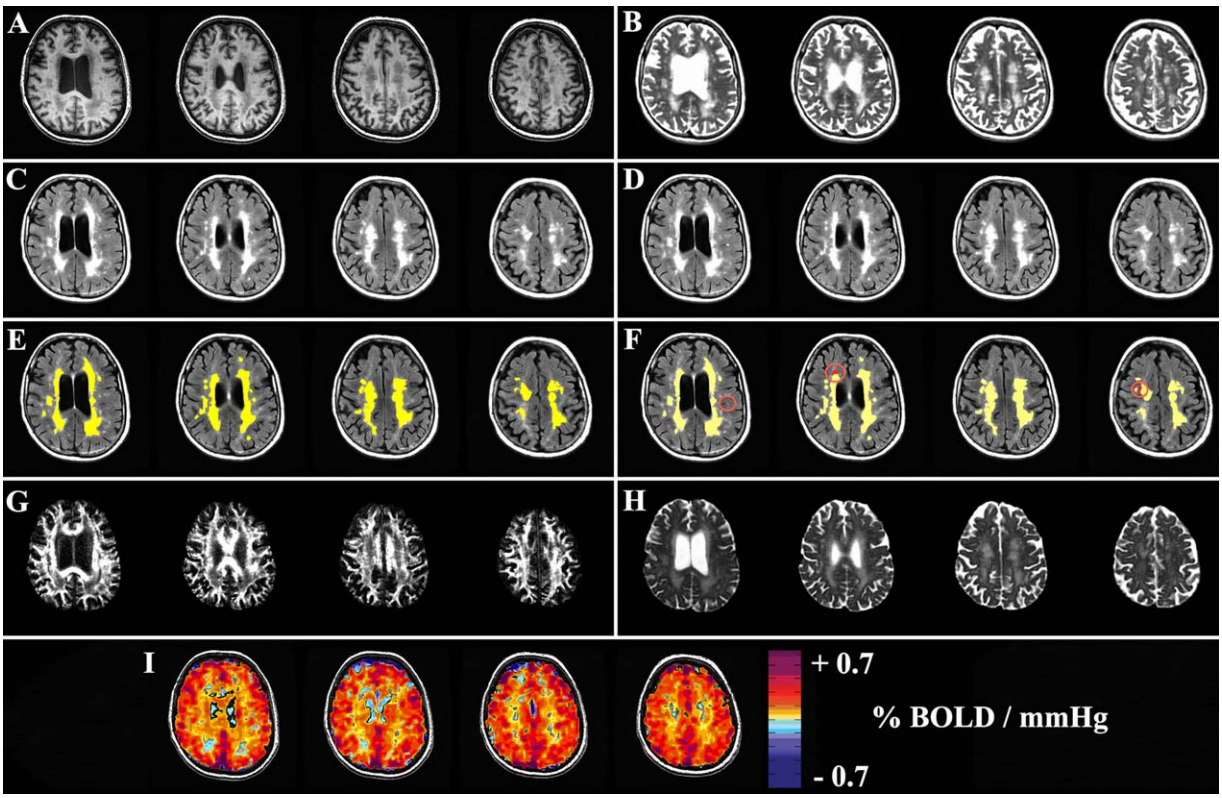

FIGURE 1: Magnetic resonance imaging metrics used in the assessment of de novo white matter hyperintensities (WMH). (A) An example of T1-weighted images from a subject with diffuse periventricular and deep WMH. (B) T2 mapping demonstrates high T2 within WMH compared to adjacent normal-appearing white matter, likely reflecting higher water content. (C) Fluid-attenuated inversion recovery (FLAIR) images demonstrate the baseline burden of disease in this subject. (D) FLAIR images on the 1-year follow-up scan of the same subject. (E) WMH from the baseline scan are highlighted in yellow. (F) WMH from baseline are highlighted in yellow and de novo WMH are highlighted in red. (G) The fractional anisotropy map of this subject demonstrates reduced anisotropy in areas of WMH. (H) The mean diffusivity map of this subject demonstrates higher diffusivity in areas of WMH. (I) The cerebrovascular reactivity (CVR) map shows reduced (negative) CVR within the WMH. BOLD = blood oxygen level–dependent.

T1-weighted images were transformed into Montreal Neurological Institute space using SPM8. The transformation matrix was applied to all other MRI metrics, transforming these maps to a standard space but retaining the native structure. AFNI was then used to identify areas of contralateral homologous NAWM corresponding to each area of WMH (Fig 2). This enables direct comparison between areas of de novo WMH and contralateral homologous NAWM, eliminating spatial location as a potential confounding factor.

Statistical Analyses

Statistical analysis was performed with SPSS 21.0 (IBM, Armonk, NY). The relationships for each MRI metric between different tissue types were compared in the following 4 ROIs: (1) WMH at baseline, (2) NAWM at baseline without progression to WMH, (3) NAWM at baseline with progression to WMH, and (4) de novo WMH on follow-up scans. For this within-subject repeated measures design, CVR was compared between the 4 ROIs listed above using a Friedman test with Dunn correction for multiple comparisons. For DTI and quantitative T2 parameters, comparisons between the 4 ROIs were performed using a repeated measures 1-way analysis of variance with FA, MD, and T2 as dependent variables and the various regions as the matched-pairs independent variable. Mauchly test was used to detect significant departures from sphericity, and the degrees of freedom were corrected using the Greenhouse–Geisser method. Results of post hoc tests were considered significant if the Bonferroni-corrected probability value was less than 0.05/(6 comparisons) = 0.008. Partial η^2 effect sizes were calculated for significant results between NAWM at baseline with versus without progression to WMH.

When accounting for spatial location by comparing NAWM that progressed to WMH versus contralateral homologous NAWM that did not progress (see Fig 2E), significance was tested with Wilcoxon matched-pairs signed ranks test for CVR measurements and 2-tailed paired t tests for DTI and T2 measurements. For these paired tests, statistical significance was assessed with $\alpha = 0.01$.

Results

The 45 subjects (age range = 50–91 years, mean age = 73.1 years; 25 males) had a mean (standard deviation [SD]) WMH volume of 26.7 (23.5) ml at baseline, and mean WMH volume of 30.0 (25.1) ml at 1-year

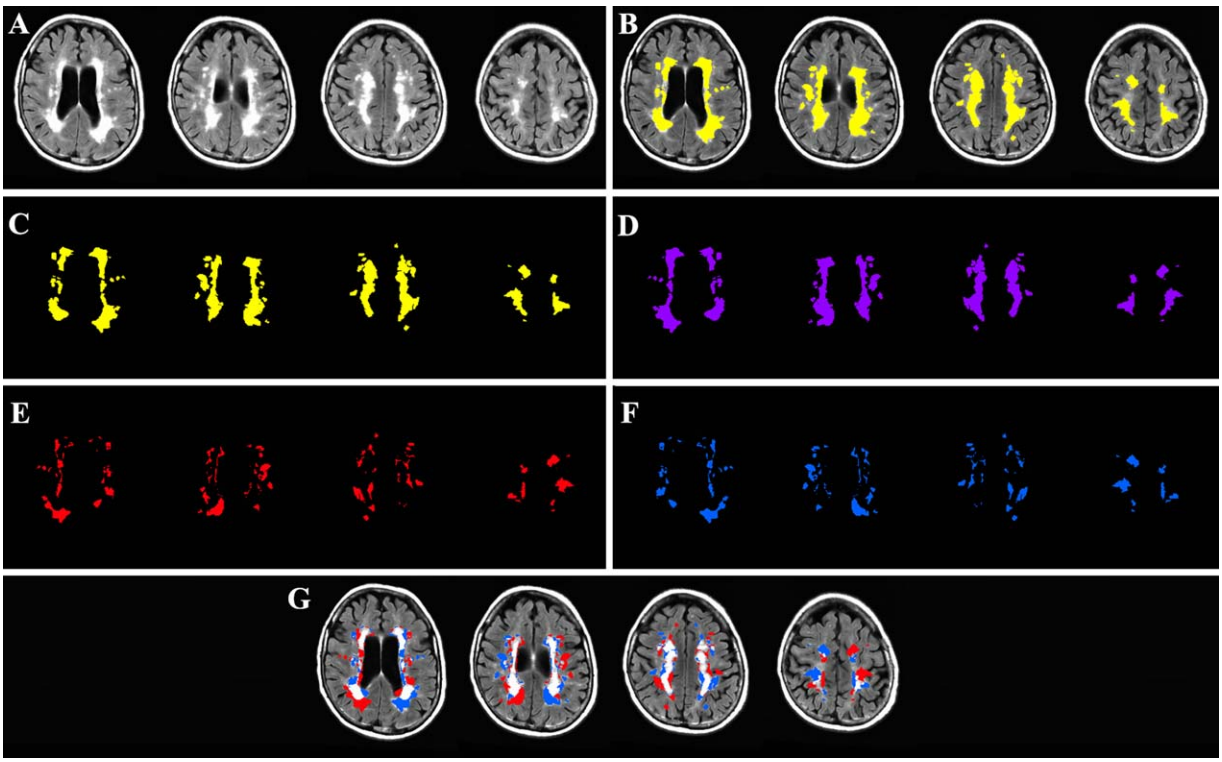

FIGURE 2: Regions used in the assessment of magnetic resonance imaging measures correcting for spatial location. (A) An example of fluid-attenuated inversion recovery (FLAIR) images from a subject with diffuse periventricular and deep white matter hyperintensities (WMH). (B) WMH highlighted in yellow. (C) WMH displayed without the underlying FLAIR image. (D) Image C left–right flipped about the y-axis in Montreal Neurological Institute coordinates while maintaining native structure. (E) Image D subtracted from C, producing normal-appearing white matter (NAWM) contralateral to WMH. (F) Image E left–right flipped about the y-axis to produce the original WMH mask so that only voxels with contralateral NAWM remain. (G) The final 2 masks, NAWM contralateral to WMH (E) and WMH containing contralateral NAWM (F) are overlaid on FLAIR images.

follow-up, yielding a WMH progression rate of 0.66 (0.60) ml/year.

The mean (SD) for each MRI parameter in each ROI is summarized in Table 2. NAWM regions that progressed to WMH were compared to NAWM regions that did not progress to WMH over the 1-year period, and the former demonstrated reduced CVR and FA, and increased MD and T2 (all $p < 0.001$).

The statistical significance of these findings remained when using the spatially corrected regions as demonstrated in Figure 2. The results of these comparisons are presented in Table 3. In this analysis, regions with bilateral disease were excluded and only WMH with contralateral NAWM were examined. Out of all white matter, the percentage of WMH that had NAWM on the contralateral side that could be used for comparison was 14.4% (8.7%). CVR and FA in NAWM that progressed to WMH were lower than in contralateral homologous NAWM that did not progress by 26.5% (23.2%) and 11.0% (7.5%), respectively, whereas MD and T2 were higher by 17.0% (8.5%) and 8.7% (7.9%), respectively (all $p < 0.001$; Fig 3). A post hoc power calculation given the observed effect size between the CVR of NAWM that progressed to WMH and contralateral NAWM was $\eta^2 = 0.275$ (large effect size).

When comparing measurements at baseline to 1-year follow-up in NAWM that progressed to WMH, CVR and FA did not change over time; MD and T2 increased on follow-up (both $p < 0.01$).

Discussion

This is the first longitudinal study to investigate the relationship between impaired cerebrovascular reactivity and the evolution of WMH. We have demonstrated that regions of NAWM that progress to WMH over time have a lower baseline CVR compared to NAWM that remains stable. We also found that these regions display subtle microstructural alterations in baseline diffusion MRI parameters, with increased MD and decreased FA. These latter measures suggest that there is a loss of tissue integrity before visible changes on conventional T1- or T2-weighted imaging. Such alterations are consistent with previous reports of abnormal diffusivity in areas of hemodynamic impairment in the NAWM of patients with intracranial[15] and extracranial steno-occlusive disease.[16] Our findings therefore suggest that areas of CVR

TABLE 2. Regional Comparison of Magnetic Resonance Imaging Metrics between Tissue Types

Metric	WMH at Baseline	NAWM at Baseline without Progression to WMH	NAWM with Progression to WMH	
			Measurements at Baseline	Measurements at Follow-up, De Novo WMH
CVR, %BOLD/mmHg	0.05 (0.05)[a]	0.12 (0.04)[b]	0.05 (0.04)[a]	0.05 (0.05)[a]
FA, unitless	0.28 (0.06)[a]	0.47 (0.05)[b]	0.31 (0.06)[a]	0.30 (0.06)[a]
MD, $\times 10^{-3}$mm^2/s	1.36 (0.11)[a]	0.85 (0.04)[b]	1.00 (0.11)[a,b]	1.08 (0.11)[a,b,c]
T2, ms	133.7 (14.4)[a]	85.3 (4.8)[b]	93.8 (9.6)[a,b]	111.7 (12.2)[a,b,c]

All comparisons with FA, MD, and T2 were made using repeated measures 1-way analysis of variance with a Bonferroni correction for multiple comparisons. CVR comparisons used Friedman test with Dunn post hoc correction. Values are expressed as mean (standard deviation).
[a]$p < 0.01$ for comparisons against NAWM at baseline without progression to WMH.
[b]$p < 0.01$ for comparisons against WMH at baseline.
[c]$p < 0.01$ between time points, NAWM with progression to WMH.
BOLD = blood oxygen level–dependent; CVR = cerebrovascular reactivity; FA = fractional anisotropy; MD = mean diffusivity; NAWM = normal-appearing white matter; WMH = white matter hyperintensities.

impairment are more prone to developing WMH, and we hypothesize that this link is due to a chronic unsuccessful competition for blood flow between regions of differing CVR.[10]

Our DTI measures are consistent with recent imaging studies that also examined the evolution of WMH and showed that reduced FA and increased MD precede progression from NAWM to WMH.[18,33] We also found prolonged T2 values in NAWM that progressed to WMH, approaching those of pre-existing WMH, although such differences were not visible on T2-weighted or PD images from baseline scans. These DTI and T2 findings indicate that pathological changes in NAWM occur before becoming visible on imaging. Prolonged T2 in NAWM may indicate signs of diffuse demyelination,[34] astrogliosis, and vasogenic edema.[35]

Our results are also consistent with animal models demonstrating cerebrovascular dysfunction months before the first histological evidence of white matter injury, including oxidative stress, blood–brain barrier disruption, oligodendrocyte loss, and glial activation.[36,37] Microglial activation and WMH have been shown to be spatially concordant in rat models of chronic hypoperfusion.[38,39] In this model, one hypothesized mechanism for WMH pathogenesis is that microglial proteases may contribute to the reduction of basement membrane components and blood–brain barrier breakdown,[40] which results in perivascular edema and leads to the development of WMH through the action of extravasated serum factors.[41]

TABLE 3. Comparison of Magnetic Resonance Imaging Metrics between NAWM at Baseline That Progresses to WMH and Their Contralateral Homologous Regions

Metric	NAWM at Baseline with Progression to WMH[b]	Contralateral Homologous NAWM
CVR, %BOLD/mmHg	0.05 (0.04)	0.08 (0.05)[a]
FA, unitless	0.2 (0.04)	0.33 (0.04)[a]
MD, $\times 10^{-3}$mm^2/s	1.25 (0.11)	1.09 (0.12)[a]
T2, ms	109.3 (12.1)	100.3 (9.64)[a]

Values are expressed as mean (standard deviation).
[a]Significance against NAWM at baseline with progression to WMH ($p < 0.01$) using a 2-way paired Student t test.
[b]Please note that this region of interest has been corrected for the spatial location confound and differs from measures found in Table 2.
BOLD = blood oxygen level–dependent; CVR = cerebrovascular reactivity; FA = fractional anisotropy; MD = mean diffusivity; NAWM = normal-appearing white matter; WMH = white matter hyperintensities.

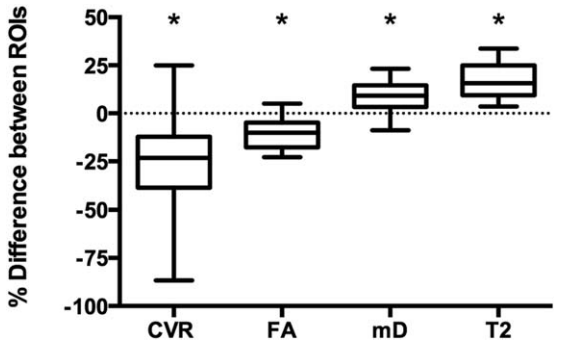

FIGURE 3: Comparison of magnetic resonance imaging parameters in regions of interest (ROIs) of normal-appearing white matter (NAWM) that progressed to white matter hyperintensities (WMH) versus spatially corresponding contralateral region of NAWM that did not develop WMH. Values are expressed as parameter values at baseline in NAWM regions that subsequently developed WMH as a percentage of the parameter value at baseline in the spatially corresponding contralateral regions that did not develop WMH. *Significant differences in paired comparison ($p < 0.01$). Error bars indicate minimum and maximum, boxes indicate the interquartile range (25th to 75th percentile), and the line within each box indicates the median. CVR = cerebrovascular reactivity; FA = fractional anisotropy; mD = mean diffusivity.

However, reduction in CVR does not necessarily indicate impaired cerebral blood flow, and may also be a consequence of increased impedance to the perivascular lymphatic drainage of interstitial fluid from the white matter.[42] In addition, a recent imaging study has shown that disruption of the blood–brain barrier may be associated with WMH and reductions in CVR; however, this study is limited in its cross-sectional design and comparison of MRI metrics between different subjects.[43] Another possibility is that increased leakage of the blood–brain barrier in NAWM combines synergistically with chronic hemodynamic impairment to precipitate WMH. Reductions in CVR may therefore result from a complex interplay of factors.

Our findings are also consistent with studies implicating hemodynamic impairment in the pathogenesis of WMH. A study looking at WMH development on a smaller time found hallmarks of acute infarction in de novo WMH.[17] It is possible that the reduced CVR in the NAWM makes this particular region prone to acute infarction. However, it remains to be determined whether acute infarcts are more likely to develop in areas with impaired CVR. One mechanism that explains how impaired CVR and infarction could lead to the development of WMH is that cerebral arteriolosclerosis, which includes elements of microatheroma, lipohyalinosis, and fibrinoid necrosis, may develop with age.[44] These changes could lead to microturbulent flow, reduce the elasticity of vessels, and result in further impairment of CVR as well as increased risk of acute infarction. Impaired CVR could also stem from endothelial dysfunction.[45] Mechanical factors such as hypertension result in damaged endothelium, which allows plasma proteins to leak into the vessel wall. Also, increased arterial pulsation related to hypertension can cause mechanical damage to veins and result in periventricular venous collagenosis. This results in intramural thickening, narrowing of the venous lumen, and reduced blood flow, and further exacerbates ischemic conditions.[46] Venous collagenosis, acute infarction, and impaired CVR may all be aggravating factors leading to white matter tissue damage and development of WMH.

We observed a mean WMH progression rate of 0.66ml/yr, consistent with the range of progression rates found in previous studies.[7,47] This progression rate was lower than expected, because a key risk factor for WMH progression is baseline WMH volume,[14,47,48] which in our cohort was 19.3ml/subject. In their longitudinal studies of community-dwelling elderly subjects with no identifiable neurological disease, Taylor et al[47] found a baseline WMH volume of 4.91 (7.01) ml/subject (mean age = 69.1 years) and Whitman et al[7] found a baseline WMH volume of 3.1 (2.5) ml/subject with corresponding progression rates of 0.76ml/yr and 0.28ml/yr, respectively. In contrast, Sachdev et al[14] found a much higher progression rate of 2.17ml/yr, with a decrease in WMH volume in 8 of 51 subjects, whereas we found a decrease in only 2 of 45 subjects. One explanation for such differences may be the differences in obliquity of the imaging plane between baseline and follow-up scans. In our study, we relied on multiple sequences with no interslice gap and automated coregistration of FLAIR, multiecho T2, PD, and conventional T2-weighted images to account for any differences in WMH volume on follow-up scans.

Limitations

Our study is limited by a relatively small sample size, which may influence the statistical power and predictive value of our prospective investigation of de novo WMH. However, a post hoc power calculation given the observed effect size between de novo WMH and contralateral NAWM CVR comparisons ($\eta^2 = 0.275$ large effect size) demonstrated that our study was adequately powered for this comparison. Another limitation is that de novo lesions represent very small tissue volumes and the metrics assessed in these regions are prone to image artifacts and to partial volume effects. These effects may influence the reliability of our measurements within de novo WMH. As well, we included only subjects with moderate–severe WMH at baseline, and therefore did not evaluate whether early/mild WMH development is

preceded by CVR impairment. Because the strongest predictor of disease progression is baseline lesion volume,[14] future studies evaluating early changes (from normal structural brain imaging to mild WMH) would likely require a larger sample size and longer follow-up interval to depict disease progression. Our study is also limited by the use of the BOLD signal as a surrogate for blood flow. However, we have previously validated our CVR methodology against measurements of cerebral blood flow obtained with arterial spin labeling in healthy controls and in patients with steno-occlusive disease.[49]

One strength of our study is our ability to accurately control $P_{ET}CO_2$ and $P_{ET}O_2$ independently of each other and of the subject's breathing pattern and minute ventilation. This ability enables us to deliver a standardized vasodilatory stimulus to all subjects. Other methods of administering a stimulus such as breath-holding or administering a fixed inspired concentration of CO_2 and O_2 (eg, "carbogen") result in considerably greater test-to-test (and subject-to-subject) variation in arterial blood gas concentrations,[50] the actual vasoactive stimuli. A submaximal stimulus may result in inaccurate CVR values, as recently described.[10,50] Our methodology reliably produced a robust vasodilatory stimulus (ie, 10mmHg change in $P_{ET}CO_2$), increasing confidence that the observed decrease in CVR represents a true hemodynamic impairment.

Conclusion

Knowledge of the sequence of events underlying the evolution of WMH has important implications for understanding lesion pathogenesis and for targeting therapeutic interventions. Our findings show that areas of NAWM that develop WMH over time have reduced CVR compared to areas of NAWM that do not. This supports the hypothesized role of chronic hemodynamic impairment in the pathogenesis of WMH.

Acknowledgment

This project was supported by the Canadian Stroke Network, Ontario Research Fund (RE 02-002), and Alternative Funding Plan for the Academic Health Sciences Centres of Ontario Innovation Fund (K.S., A.P.C., J.P., J.C., O.S., J.D., D.M.M., J.A.F., S.E.B., D.J.M.). The Sunnybrook brain laboratory received support from the Heart and Stroke Foundation Canadian Partnership for Stroke Recovery and LC Campbell Foundation (S.E.B.).

We thank the TWH and SHSC RespirAct technologists, A. Battisti-Charbonney and D. Pham, as well as the MRI technologists, K. Ta and E. Hlasny; D. Crane (MacIntosh laboratory manager) and A. Ganda (psychometrist/research coordinator) for enabling the Sunnybrook data acquisition, which required availability after hours on weekends; A. McNeely and C. Berezuk, Sunnybrook brain laboratory imaging analysts, for identifying areas of WMH and lacunas for the Sunnybrook data set; and C. Scott, Sunnybrook brain laboratory manager, for facilitating training and analysis using the Lesion Explorer pipeline.

Author Contributions

The study was conceived and designed by K.S., A.P.C., D.M.M., J.D., J.A.F., S.E.B., and D.J.M.; K.S. and O.S. contributed to data acquisition; all authors contributed to data analysis and interpretation; K.S., J.C., A.P.C., and J.D. drafted the manuscript and figures.

Potential Conflicts of Interest

J.A.F and D.J.M. are coinventors of the RespirAct, a device used in this study. J.D., J.A.F., and D.J.M. hold shares in Thornhill Research, a University of Toronto/University Health Network–related company that provides the RespirAct, and will receive royalties should the RespirAct become a commercial product.

References

1. Hachinski VC, Potter P, Merskey H. Leuko-araiosis: an ancient term for a new problem. Can J Neurol Sci 1986;13(4 suppl):533–534.
2. Wardlaw JM, Smith EE, Biessels GJ, et al. Neuroimaging standards for research into small vessel disease and its contribution to ageing and neurodegeneration. Lancet Neurol 2013;12:822–838.
3. Verdelho A, Madureira S, Moleiro C, et al. White matter changes and diabetes predict cognitive decline in the elderly: the LADIS study. Neurology 2010;75:160–167.
4. Schmidt R, Schmidt H, Kapeller P, et al. The natural course of MRI white matter hyperintensities. J Neurol Sci 2002;203–204:253–257.
5. Gunning-Dixon FM, Raz N. The cognitive correlates of white matter abnormalities in normal aging: a quantitative review. Neuropsychology 2000;14:224–232.
6. Malmstrom TK, Morley JE. The frail brain. J Am Med Dir Assoc 2013;14:453–455.
7. Whitman GT, Tang Y, Lin A, Baloh RW. A prospective study of cerebral white matter abnormalities in older people with gait dysfunction. Neurology 2001;57:990–994.
8. de Leeuw FE, de Groot JC, Achten E, et al. Prevalence of cerebral white matter lesions in elderly people: a population based magnetic resonance imaging study. The Rotterdam Scan Study. J Neurol Neurosurg Psychiatry 2001;70:9–14.
9. Launer LJ, Berger K, Breteler MM, et al. Regional variability in the prevalence of cerebral white matter lesions: an MRI study in 9 European countries (CASCADE). Neuroepidemiology 2006;26:23–29.
10. Sobczyk O, Battisti-Charbonney A, Fierstra J, et al. A conceptual model for CO(2)-induced redistribution of cerebral blood flow with experimental confirmation using BOLD MRI. Neuroimage 2014;92:56–68.

11. Spano VR, Mandell DM, Poublanc J, et al. CO2 blood oxygen level-dependent MR mapping of cerebrovascular reserve in a clinical population: safety, tolerability, and technical feasibility. Radiology 2013;266:592–598.
12. Uh J, Yezhuvath U, Cheng Y, Lu H. In vivo vascular hallmarks of diffuse leukoaraiosis. J Magn Reson Imaging 2010;32:184–190.
13. Mandell DM, Han JS, Poublanc J, et al. Selective reduction of blood flow to white matter during hypercapnia corresponds with leukoaraiosis. Stroke 2008;39:1993–1998.
14. Sachdev P, Wen W, Chen X, Brodaty H. Progression of white matter hyperintensities in elderly individuals over 3 years. Neurology 2007;68:214–222.
15. Conklin J, Fierstra J, Crawley AP, et al. Impaired cerebrovascular reactivity with steal phenomenon is associated with increased diffusion in white matter of patients with Moyamoya disease. Stroke 2010;41:1610–1616.
16. Conklin J, Fierstra J, Crawley AP, et al. Mapping white matter diffusion and cerebrovascular reactivity in carotid occlusive disease. Neurology 2011;77:431–438.
17. Conklin J, Silver FL, Mikulis DJ, Mandell DM. Are acute infarcts the cause of leukoaraiosis. Brain mapping for 16 consecutive weeks. Ann Neurol 2014;76:899–904.
18. de Groot M, Verhaaren BF, de Boer R, et al. Changes in normal-appearing white matter precede development of white matter lesions. Stroke 2013;44:1037–1042.
19. Fazekas F, Chawluk JB, Alavi A, et al. MR signal abnormalities at 1.5 T in Alzheimer's dementia and normal aging. AJR Am J Roentgenol 1987;149:351–356.
20. Kisilevsky M, Hudson C, Mardimae A, et al. Concentration-dependent vasoconstrictive effect of hyperoxia on hypercarbia-dilated retinal arterioles. Microvasc Res 2008;75:263–268.
21. Ito S, Mardimae A, Han J, et al. Non-invasive prospective targeting of arterial P(CO2) in subjects at rest. J Physiol 2008;586(pt 15):3675–3682.
22. Fierstra J, Sobczyk O, Battisti-Charbonney A, et al. Measuring cerebrovascular reactivity: what stimulus to use? J Physiol 2013; 591(pt 23):5809–5821.
23. Slessarev M, Han J, Mardimae A, et al. Prospective targeting and control of end-tidal CO2 and O2 concentrations. J Physiol 2007; 581(pt 3):1207–1219.
24. Fisher JA, Iscoe S, Duffin J. Sequential gas delivery provides precise control of alveolar gas exchange. Respir Physiol Neurobiol 2016;225:60–69.
25. Vesely A, Sasano H, Volgyesi G, et al. MRI mapping of cerebrovascular reactivity using square wave changes in end-tidal PCO2. Magn Reson Med 2001;45:1011–1013.
26. Cox RW. AFNI: software for analysis and visualization of functional magnetic resonance neuroimages. Comput Biomed Res 1996;29: 162–173.
27. Miller AJ, Joseph PM. The use of power images to perform quantitative analysis on low SNR MR images. Magn Reson Imaging 1993;11:1051–1056.
28. Smith SM, Jenkinson M, Woolrich MW, et al. Advances in functional and structural MR image analysis and implementation as FSL. Neuroimage 2004;23(suppl 1):S208–S219.
29. Jenkinson M, Bannister P, Brady M, Smith S. Improved optimization for the robust and accurate linear registration and motion correction of brain images. Neuroimage 2002;17:825–841.
30. Smith SM. Fast robust automated brain extraction. Hum Brain Mapp 2002;17:143–155.
31. Ramirez J, Scott CJ, McNeely AA, et al. Lesion Explorer: a video-guided, standardized protocol for accurate and reliable MRI-derived volumetrics in Alzheimer's disease and normal elderly. J Vis Exp 2014(86).
32. Ramirez J, Gibson E, Quddus A, et al. Lesion Explorer: a comprehensive segmentation and parcellation package to obtain regional volumetrics for subcortical hyperintensities and intracranial tissue. Neuroimage 2011;54:963–973.
33. Maillard P, Carmichael O, Harvey D, et al. FLAIR and diffusion MRI signals are independent predictors of white matter hyperintensities. AJNR Am J Neuroradiol 2013;34:54–61.
34. Haughton VM, Yetkin FZ, Rao SM, et al. Quantitative MR in the diagnosis of multiple sclerosis. Magn Reson Med 1992;26:71–78.
35. Armspach JP, Gounot D, Rumbach L, Chambron J. In vivo determination of multiexponential T2 relaxation in the brain of patients with multiple sclerosis. Magn Reson Imaging 1991;9:107–113.
36. Shibata M, Ohtani R, Ihara M, Tomimoto H. White matter lesions and glial activation in a novel mouse model of chronic cerebral hypoperfusion. Stroke 2004;35:2598–2603.
37. Ihara M, Tomimoto H. Lessons from a mouse model characterizing features of vascular cognitive impairment with white matter changes. J Aging Res 2011;2011:978761.
38. Wakita H, Tomimoto H, Akiguchi I, Kimura J. Dose-dependent, protective effect of FK506 against white matter changes in the rat brain after chronic cerebral ischemia. Brain Res 1998;792:105–113.
39. Farkas E, Donka G, de Vos RA, et al. Experimental cerebral hypoperfusion induces white matter injury and microglial activation in the rat brain. Acta Neuropathol 2004;108:57–64.
40. Hamann GF, Okada Y, Fitridge R, del Zoppo GJ. Microvascular basal lamina antigens disappear during cerebral ischemia and reperfusion. Stroke 1995;26:2120–2126.
41. Akiguchi I, Tomimoto H, Suenaga T, et al. Blood-brain barrier dysfunction in Binswanger's disease; an immunohistochemical study. Acta Neuropathol 1998;95:78–84.
42. Huang YH, Zhang WW, Lin L, et al. Could changes in arterioles impede the perivascular drainage of interstitial fluid from the cerebral white matter in leukoaraiosis? Neuropathol Appl Neurobiol 2010;36:237–247.
43. Munoz Maniega S, Chappell FM, Valdes Hernandez MC, et al. Integrity of normal-appearing white matter: influence of age, visible lesion burden and hypertension in patients with small-vessel disease. J Cereb Blood Flow Metab (in press).
44. Xiong YY, Mok V. Age-related white matter changes. J Aging Res 2011;2011:617927.
45. Knottnerus IL, Ten Cate H, Lodder J, et al. Endothelial dysfunction in lacunar stroke: a systematic review. Cerebrovasc Dis 2009;27: 519–526.
46. Topakian R, Barrick TR, Howe FA, Markus HS. Blood-brain barrier permeability is increased in normal-appearing white matter in patients with lacunar stroke and leucoaraiosis. J Neurol Neurosurg Psychiatry 2010;81:192–197.
47. Taylor WD, MacFall JR, Provenzale JM, et al. Serial MR imaging of volumes of hyperintense white matter lesions in elderly patients: correlation with vascular risk factors. AJR Am J Roentgenol 2003;181:571–576.
48. Schmidt R, Petrovic K, Ropele S, et al. Progression of leukoaraiosis and cognition. Stroke 2007;38:2619–2625.
49. Mandell DM, Han JS, Poublanc J, et al. Mapping cerebrovascular reactivity using blood oxygen level-dependent MRI in patients with arterial steno-occlusive disease: comparison with arterial spin labeling MRI. Stroke 2008;39:2021–2028.
50. Fisher JA. The CO2 stimulus for cerebrovascular reactivity: fixing inspired concentrations vs. targeting end-tidal partial pressures. J Cereb Blood Flow Metab 2016;36:1004–1011.